Ocean Engineering 230 (2021) 109059

Contents lists available at ScienceDirect

Ocean Engineering

journal homepage: www.elsevier.com/locate/oceaneng

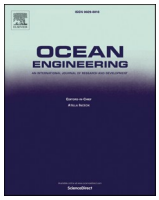

Making sense of speed effects on ice crushing pressure-area relationships in IACS ice-strengthening rules for ships

Ekaterina Kim *, Jørgen Amdahl, Xintong Wang

Norwegian University of Science and Technology, Otto Nielsens vei 10, Trondheim, Norway

ARTICLE INFO

Keywords:
Shipping
IACS
Ice loads
Crushing
Pressure-area
Speed-effects

ABSTRACT

Arctic shipping fleet expansion is anticipated in the future. However, future refinements in the understanding of ice loads on larger ships are needed to achieve a better structural design with reduced steel weight. Published rules for the strength of ships are derived from semi-empirical methods and calibrated with limited full-scale measurements on small ships. In 2015, the Lloyd's Register pointed out that for independent navigation of larger ships in heavier ice conditions, steel weight increases exponentially with the ice thickness, which negatively affects the economy of ships' operations.

Motivated by this statement, the objective of this paper is to address uncertainty in rule-derived ice loads using an ice mechanics point of view. The focus is on the local ice crushing loads and the vessel speeds in the Unified Requirements for Polar Class Ships of the International Association of Classification Societies (IACS).

In this work, we attempt to relate the IACS speed-dependent ice pressure-area relationships to the simplified principles of ice mechanics coupled with structural design considerations. This relation enables us to better understand uncertainties in the rule loads for larger ships, which is essential to address the economy of Arctic ships' operations. The results of this study showed that the choice of parameters in IACS ice crushing loads for larger vessels with higher ice classes (PC1) has high uncertainty and the upper limit values are greater than those predicted by the ice mechanics approach.

1. Introduction

The Arctic has experienced an increase in passenger cruise voyages and marine export shipping of nonrenewable natural resources from coastal regions and the interior. One of the main engineering challenges is how to design a safe and economically efficient ship structure that is capable of operating in ice-covered waters. In ship-design practices, it is common to specify ice loads in the form of pressures, which are used to design shell plating and frames.

It is traditionally assumed (Johansson, 1967) that a larger, more powerful ship is more likely to encounter stronger ice. As a result, the design loads increase exponentially as the ship size increases, and higher ice class ships are less efficient to operate and more expensive to build (Lloyd's Register, 2015).

The classification societies provide guidelines for the strengthening of ice-going ships. Finnish Swedish Ice Class Rules (FSICR) are often accepted as an industry standard for designing ships for first-year ice environments (Riska and Kämä, 2011), whereas the International Association of Classification Societies (IACS) Polar Class Rules represent the latest scientific and engineering thinking on how to dimension a ship structure that operates in areas with multiyear ice and glacier ice features. When determining ice loads on ice-going ships, rule developers traditionally rely on semi-empirical methods, which are calibrated with full-scale measurements. The data sets that were employed for calibration of the IACS rules are obtained from existing small icebreakers and moderately sized icebreaking cargo ships. To account for the uncertainty of larger ships, which exceed the calibration range, the assumed design ice pressures tend to become conservative. In the future, as the feedback from ships in operation (in the form of ice damage) accumulates and as the knowledge about ice loads improves, the rule formulations might be updated.

However, collecting full-scale data for larger vessels and higher ice classes is a challenge because none of the newly built icebreaking cargo vessels has PC2 and/or PC1 classes. This lack of PC2 and PC1 icebreaking cargo vessels, combined with the recognition that full-scale data on ice damage for larger ships are scarce (if any data are publicly available), lead us to address the uncertainties in rule-derived ice loads from an ice mechanics point of view coupled with a structural design

* Corresponding author.
E-mail addresses: ekaterina.kim@ntnu.no (E. Kim), jorgen.amdahl@ntnu.no (J. Amdahl), xintong.wang@ntnu.no (X. Wang).

https://doi.org/10.1016/j.oceaneng.2021.109059
Received 22 June 2020; Received in revised form 21 February 2021; Accepted 18 April 2021
Available online 7 May 2021

perspective.

The focus of this study is local ice crushing loads in the Unified Requirements for Polar Class Ships of the International Association of Classification Societies (IACS). The local ice crushing loads are specified in terms of the pressures in the corresponding areas that are used to design shell plating and frames. First, we rederive the ice pressure-area relationships using simplified principles of ice mechanics reported by Schulson and Duval (2009). Second, we relate the derived pressures to those from the IACS rules that account for the associated uncertainties. We aim to highlight the IACS underlying assumptions based on some principles of ice mechanics and to achieve a better understanding of the uncertainties and conservatism (if any) in the modern rule formulations. An improved understanding of the uncertainties in the IACS ice loads is essential when the economy of Arctic ships' operations is addressed.

2. Pressure-area relationships

The ice pressure-area (PA) relationships fall into three categories: *process curves* (termed by Frederking 1998), *spatial-distribution curves* (termed by Frederking 1999) and characteristic (or design) curves. The latter category of curves is often viewed in the context of local or global ice loads and probabilistic or deterministic approaches to design. A process PA curve describes the process of a structure that penetrates an ice feature or the process of an ice feature that hits a structure. This curve is a continuous plot of the variation in the average pressure versus the total contact area during an ice-structure interaction process. A spatial-distribution PA curve characterizes the average pressure on subareas of various sizes within a total contact area at an instant in time. To establish this curve, knowledge of the true contact area and pressure distribution at each time instant is required.

Empirical data reported in Timco and Sudom (2013) indicate that for stationary structures (lighthouses, bridge-piers, offshore caisson structures, etc.), the global and local pressures depend on the loading speed, ice failure mode, and aspect ratio (width of the structure relative to the ice thickness), as well as ice properties (temperature, salinity, density, and grain structure and orientation). The most common way of expressing a local PA relationship is the power-law expression $p = CA^q$, where p is the pressure over a corresponding area A, and C and q are empirical constants. The exponent q is typically a negative number between 0 and –1.

For ships (moving structures), there have been several experimental studies on how different conditions (vessel speed, ice thickness, and season of operation) affect global and local loads and the interpretation of full-scale records to identify extreme ice loads during service operations and benchmarking of ice class selection (e.g., Glen and Blount, 1984; Kujala and Vuorio, 1986; St John et al., 1990; 1995; Kotisalo and Kujala, 1999; Frederking, 2000; Hänninen et al., 2001; Matsuzawa et al., 2010; Iyerusalimskiy et al., 2011; Kwon et al., 2015; Kim et al., 2016; Jo et al., 2018).

Dedicated ship trials and voyages include, e.g., SS Manhattan voyages, 1969-70; CCGS Louis S. St. Laurent voyages, 1980 and 1994; Canmar Kigoriak voyages, 1981 and 1983; Polar Sea voyages 1982, 1983, 1984, 1985 and 1986; MV Arctic voyage, 1984 (see, e.g., interpretations of data by Ralph, 2016); Swedish Icebreaker Oden Arctic Ocean Expedition, 1991; NSF R/V Nathaniel B. Palmer ice trials, 1992; Icebreaker Sisu voyages 1979-85; MT Uikku voyage, 1998; SA-15 Igarka and Kapitan Danilkin voyages in 1998; USCGC Healy Trials, 2000; CCGS Terry Fox bergy bit impact study; 2001 KV Svalbard ice trials in 2006, 2007, and 2011; PSRV S.A. Agulhas II voyage 2012; ARAON ice tests in 2010, 2012, and 2016; Arc4−Arc7 tankers ice trials and voyages, 2009–2017.

There is a discrepancy in the interpretation of the data from ships, i.e., the data from Nataniel B. Palmer (St John and Minnick, 1995), ARAON (Kim et al., 2014), and Terry Fox (Ritch et al., 2008) do not show a distinct dependency of ice pressure on ship speed, whereas data from ARAON in 2016 indicate that the pressure increases with an increase in ship speed (refer to Fig. 8 in Cho and Choi (2019)). This discrepancy in the interpretation of full-scale data reflects the complexity of the ice-structure interaction even in 'controlled' ship-based tests when the ice parameters (mechanical and geometrical) have been recorded. Understanding the pressure-area relationships from full-scale operational data of a merchant vessel is even more challenging, because some ice parameters cannot be measured while the ship is moving, and the contact geometry between the ship and the ice is constantly changing, which introduces a constant interplay between crushing and bending failure. Furthermore, the operator's perception of ice conditions influences handling of the vessel in ice (e.g., vessel speed, angle of attack), and thus, affects the ice loads. Despite these difficulties, *interpretations that are based on full-scale data* (i.e., semi-empirical approaches) *provide the best estimates of ice pressures on ship and offshore structures*.

Probabilistic interpretations of ship ram data with first year ice, multiyear ice and bergy bits for local design can be obtained from the international standard for offshore structures ISO 19906, Sec. A8.2.5.3. The sections below briefly review the semi-empirical ice crushing load model in IACS ship rules and less-known alternative deterministic formulations.

3. Background to IACS's ice loads

This section briefly presents the underlying assumptions behind the design ice crushing loads in the IACS Unified Requirements (IACS UR) for Polar Class ships (Section I2.3), whereas detailed information on this topic is provided in Daley (2000) and IACS (2019). The design scenario is an oblique collision with a large ice floe that has a 150° front angle. Ice loads on a ship's hull are characterized by an average pressure (p) that is uniformly distributed over a rectangular load patch of height (b) and width (w) and dependent on the ice category, hull angles and ship displacement. An energy-based approach (Popov et al., 1967) combined with empirical pressure-area relationships is adopted for the ice load. The kinetic energy of the ship is equated to the ice-crushing energy, which is determined by integrating the ice force over the penetration depth. The ice force is calculated by integrating the ice crushing pressure (p_{cr}) over the nominal contact area (A). A process pressure–area relationship (Eq. (1)) is assumed, where P_0 is the ice strength factor (reference ice pressure) which is class-dependent, and the exponent q (*ex* in Daley, 2000) is a constant, i.e., average pressure decreases with the nominal (projected) contact area. P_0 and q are estimated from measured data for ice interaction with ship hulls. The constant q is set to -0.1 for all ice classes independent of a vessel's speed.

$$p_{cr} = P_0 A^q \quad [1]$$

For an angular ice floe, the nominal contact area (A) is triangular-shaped (Fig. 1). To simplify the calculations, a rectangular contact area (load patch) with the same aspect ratio (a_r) and area is utilized. The effect of local ice edge fractures (spalls) is treated by assuming a reduction in the size of the nominal contact area while maintaining a constant aspect ratio and total force. This area reduction in size (A_{red}) is given by the following equation, where the spalling parameter ω (*wex* in Daley, 2000) is set to 0.7 and is independent of the ice class or speed, and β is the frame angle from the vertical (β' in Daley, 2000):

$$A_{red} = \frac{A^{\omega}}{a_r^{1-\omega}}; a_r = 7.46\sin(\beta) \geq 1.3 \quad [2]$$

At the end of the collision, i.e., when all kinetic energy is dissipated by ice deformation, the ice crushing pressure, height and width of the load patch are calculated. The sensitivity analysis presented in Kim and Amdahl (2016) shows that the values of the exponent in the process pressure–area relationship (q) and spalling characteristic (ω) are the most influencing parameters for the ice pressure values. For each ice class, assumptions are made regarding the vessel's speed that underlies the P_0 value in Eq. (1) and the bending failure. Furthermore, as noted in

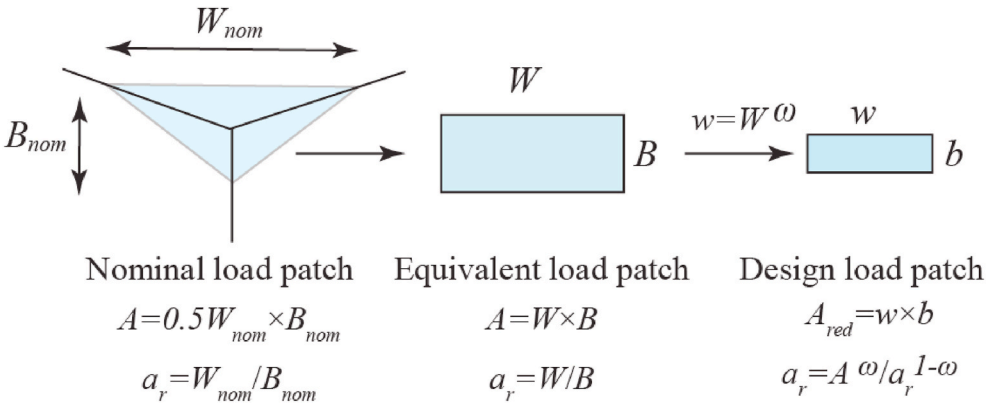

Fig. 1. Area modifications that underlie IACS Section I2.3.

IACS (2019), the assumption of the triangular-shaped area is valid if the vertical projection of the contact area is less than the assumed thickness of the ice and if this thickness has a physical meaning for the crushing impact scenario in the IACS UR. For a vertical (or nearly vertical) structure and not fulfilling the above criteria, when the effect of ice bending failure is minimized, a_r is set to 3.6, and the design ice pressure depends on the location w.r.t to the bow, ice class, and vessel's displacement. The design pressure formulations are given in IACS UR (Section I2.3.2.2) and omitted herein.

4. Alternative deterministic formulations

This section presents two less known but alternative deterministic approaches to local ice pressures. The first approach is the modified hydrodynamic model of ice impact (Appolonov et al., 2011, 2018), and the second approach is the method of the Russian Maritime Register of Shipping (RMRS) for the calculation of ice loads on structures with nonstandard hull shapes (RMRS, 2017). The following paragraphs briefly outline the approaches, whereas additional details are given in the Appendix.

The *modified hydrodynamic model* (MHDM), named by Appolonov et al. (2018), originates from the work of Kurdyumov and Kheisin (1974) and Kurdyumov et al. (1980) in an attempt to address criticism of past works; see for example, Riska (2018). The MHDM replaces an earlier assumption that the pressure is proportional to the crushed layer thickness (parabolic spatial pressure distribution) with a set of additional conditions that yield a conceptually different pressure profile over the loading height. At the center of the contact zone ($x \le b_0/2$, where x is the coordinate with the origin at the center of the loading height; b_0 is the width of the high-pressure zone), the solution of the extrusion model (i.e., infinite pressure) is replaced by a constant pressure (p_m). For $b_0/2 < x \le b/2$, the solution of the viscous ice extrusion applies and is given as follows:

$$p(x) = \left[p_m - \frac{2AV}{b}\left(\frac{b}{b_0} - 1\right)\right] \frac{\left(\frac{b}{2x}\right)^2 - 1}{\left(\frac{b}{b_0}\right)^2 - 1} + \frac{2AV}{b}\left(\frac{b}{2x} - 1\right) \quad [3]$$

In Eq. (3), $p(x)$ is the pressure profile over the loading height b equal to the ice thickness; V is the normal speed; $A = 3\mu/K^3$ (μ is the dynamic viscosity of crushed ice in the intermediate layer (h) and K is the proportionality coefficient between x and the crushing layer thickness ($h = Kx$). For details of the derivation of Eq. (3), refer to the Appendix. The resulting pressure profile is illustrated in Fig. 7 (sketch on the right-hand side).

In addition to the MHDM, a purely empirical approach exists in the engineering community (RMRS, 2017). This approach assumes that the contact pressure is a function of the uniaxial compressive strength and depends on ice temperature, salinity, density, ice loading direction, ice age (first-year ice, multiyear ice) and ice type (level ice, deformed ice). Different temperature and salinity profiles through the ice thickness are assumed and depend on the snow depth, ice age/type and time of the year (winter-spring navigation, summer-autumn navigation). A hypothetical scenario is provided in the Appendix to illustrate the methodology.

Similar to the IACS procedure, both the MHDM and RMRS adopt Popov's energy-based approach, which is proposed for the ice load calculation. The kinetic energy of the ship is equated to the ice-crushing energy, which is determined by integrating the ice force over the penetration depth. The ice force is calculated by integrating the ice crushing pressure over the nominal contact area. The effect of local ice edge fractures (spalls) is treated by assuming a reduction in the size of the nominal contact area. Furthermore, RMRS (Eq. 4.35) includes an exponential softening of the average contact pressure with an increase in the contact area. The latter assumption resembles the pressure-area curve (Eq. (1)) of the IACS.

At the end of the collision, i.e., when all kinetic energy is dissipated by ice deformation, the ice crushing pressure, height, and width of the ice-load patch are calculated using either the MHDM or the RMRS approach.

The available literature on the MHDM lacks clear guidance about how to set up the p_m, nominal contact area A, and b_0 values for different ice classes, which hinders a quantitative comparison (if not impossible). Further, we focus on addressing the uncertainties in the empirical constant q, ice strength factor P_0, and ship' s speed (V).

5. Reconstruction of pressure-area relationships: ice mechanics

Ice is a complex material. Its response to compressive loading depends on many parameters, such as the loading rate, loading direction, ice type, grain size, temperature, degree of confinement, and loading history (damage state). Details on the ice constitutive response are provided in, e.g., Schulson and Duval (2009). Ductile failure is dominant with low loading rates, high ice temperatures, and high degrees of confinement. Brittle failure dominates with high loading rates, low temperatures and low degrees of confinement. This dominance of ductile or brittle failure will influence the spatial pressure distribution over the contact area, even when the other parameters of ice-structure interaction are constant. Furthermore, the confinement raises the failure stress (σ_1) with the effect being greater within the regime of brittle behavior.

The following approach (simplified 'mechanics' method) attempts to simultaneously account for the effects of ice confinement and the loading rate using a deterministic viewpoint. For a reference temperature of −10 °C, the different loading speed regimes (ductile and brittle) give presumably different spatial pressure distributions (as illustrated in

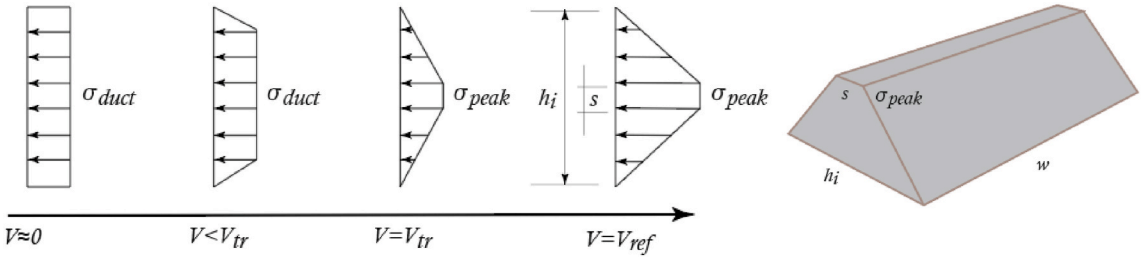

Fig. 2. Schematic of the spatial pressure-area distribution as a function of speed (Eqs. (4a)-(4d)). Representation of the shape of the ice pressure distribution resembles empirical pressure distributions reported by Sodhi et al. (1998) in Figs. 7 and 8.

Fig. 2). The pressure is viewed as the σ_1 component of the stress tensor. The pressure-area curves are reconstructed from spatial pressure distributions (shown in Fig. 2). In the pressure-area curve, the pressure is treated as an average pressure over the contact area. We take a conservative approach and do not consider the softening behavior of ice that was explained in Kim and Schulson (2015).

This section presents a derivation of the pressure-area curves as a function of impact speed. The derivations are per unit width (w) of the contact area for contact heights (h_i) larger than 0.1 m.

At low loading rates $V \leq V_{tr}$ (vessel speeds below a certain threshold), we assume a transition from fully ductile ice failure, where the pressure is uniformly distributed over the contact area to predominantly brittle failure with high pressures zones that are concentrated in the center of the contact area. The high-pressure zones are zones where confinement is high enough to suppress Coulombic faulting and activate instead plastic faulting with the nonzero deviatoric component of the stress tensor. At high loading rates (vessel speeds over a certain threshold), brittle failure dominates and the peak pressure linearly increases with the loading rate and depends on the degree of confinement, which is assumed to be the highest in the central zone. Away from this zone, the pressure decreases linearly and reaches zero at the periphery of the contact area (Fig. 2). In addition, we consider the universal behavior of brittle materials, including the failure parameters given in (Renshaw and Schulson, 2001).

Governing equations

$$p_{cr} = \begin{cases} \sigma_{duct} & V \leq V_{tr} \\ \dfrac{\sigma_{peak}}{h_i}\left(\dfrac{s+h_i}{2}\right) & V > V_{tr} \end{cases} \quad [4a]$$

$$\sigma_{peak} = \left(1 + \frac{V}{V_{ref}}\frac{\sigma_{conf} - \sigma_{duct}}{\sigma_{duct}}\right)\sigma_{duct} \quad [4b]$$

Table 1
Model parameters for ice impact.

Parameter	Value	Reference/Comment
Ductile to brittle transition V_{tr}	2 (knots)	Min attainable speed in ice
Fracture Toughness (K_{IC})	100 kPa $m^{0.5}$	Schulson and Duval (2009)
Characteristic grain size c	10 mm	Representative number
Ice temperature	−10 °C	Representative value
Unified constant U	10	Renshaw and Schulson (2001)
Ductile strength σ_{duct}	3[a] MPa	Pond Inlet tests ($V \to 0$), Geotech Arctic Services (1985)
Reference speed V_{ref}	20 (knots)	Open water speed
s (laboratory sample size)	0.1 m	Schulson and Duval (2009)

[a] For comparison, 2.4 MPa is assumed to be the uniaxial horizontal compressive strength of the Baltic ice (Riska, 2018), and approximately 2.0 MPa is the unconfined uniaxial compressive strength of freshwater columnar S2 ice measured in the laboratory at −10 °C and a strain rate of 10^{-5} 1/s (Schulson and Duval, 2009). The ice can be confined locally across columns; thus, its ductile strength will increase, whereas the strength will decease with an increase in salinity.

$$\sigma_{conf} = U\frac{K_{IC}}{\sqrt{c}} \quad [4c]$$

$$s = \begin{cases} h_i - \dfrac{h_i - s}{V_{tr}}V & V \leq V_{tr} \\ s & V > V_{tr} \end{cases} \quad [4d]$$

p_{cr} is the average ice crushing pressure per unit width of the contact area for the contact height (h_i); V_{tr} – ductile to brittle transition speed; V_{ref} – reference speed; σ_{conf} – upper limit of σ_{peak} at V_{ref}. K_{IC} – fracture toughness; U – unified constant, c – characteristic grain size; σ_{duct} – ductile ice strength; V – vessel's speed; s and σ_{duct} – parameters of the spatial pressure distribution, as shown in Fig. 2.

A summary of the underlying model parameters is given in Table 1.

6. Results

In this section results from the ice mechanics model (this study, Section 4) were related to the IACS UR pressure-area relationships (I2.3). Global pressures (or process pressure-area curves) and local (or design) pressures were plotted for different vessel speeds (or ice classes) and sizes.

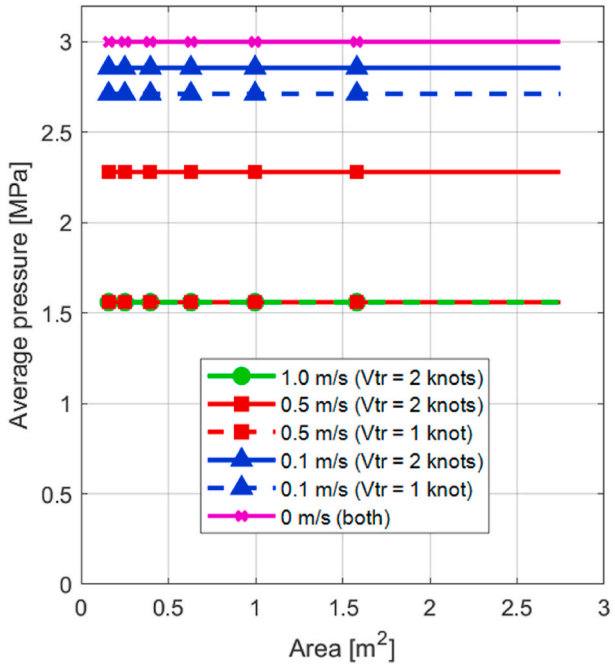

Fig. 3. Illustration of pressure-area relationships in the 'ductile' regime given by the 'mechanics model'. Vessel speeds of → 0.0, 0.1, 0.5 for different transition speed V_{tr} = 1 knot (dashed lines), and V_{tr} = 2 knot (solid lines). The pressure is associated with a full ice thickness of 2.5 m.

Fig. 3 presents the process pressure-area relationship for the ductile regime (Equation (4a) – 4d for $V \leq V_{tr}$ and the contact height equal to the ice thickness, $h_i = 2.5$ m). To minimize the effect of bending, the interaction between a large ice floe (150° front angle) and a vertical structure ($\beta = 0°$) has been considered. The change in pressure with area in the ductile regime is negligible because the pressure is evenly distributed over the contact area. When the velocity approaches zero, the mechanics model (this study) gives a maximum pressure of 3.0 MPa, which is the value of the ductile strength used in the model. When the velocity increases in the ductile regime, the average pressure decreases owing to the uneven character of the pressure distribution over the contact area. For $0 < V \leq V_{tr}$, if strain-rate hardening is included within the ductile regime, the average pressure values in Fig. 3 are expected to be higher.

Fig. 4 presents the pressure-area relationship derived using the 'mechanics' model and the process pressure-area relationship assumed by IACS for PC1–PC3 and PC7 (Daley, 2000; Equation a9). For the purpose of comparison, in the 'mechanics' approach, the contact pressures, which are averaged over the corresponding contact areas, were calculated following the procedure presented in Annex A (Equations a5 – a9 and a23 – a26) by Daley (2000), except that a9 (Equation (1)) was replaced by Equation (4a)–4d (with parameters from Table 1). The parameter $\beta = 10.1°$—a validity range of the Daley formulation—has been applied. Only ice crushing at −10 °C was considered. As a conservative estimate, the highest local pressures were assumed in the middle of the contact height.

Except for PC1 (contact areas < 0.3 m^2), for the considered areas (from 0.1 m^2 to 3.0 m^2), the 'mechanics' model with the parameters in Table 1 always gives a higher crushing pressure than that assumed by IACS UR (ice crushing loads in Section I2.3.2.1). This result is reasonable as the bending effect, which is present for frame angles of 10° and is not included in the 'mechanics' model. Note that the gap between the pressure-area curves for two adjacent Polar Classes increases (due to the uncertainty) from lower class vessels to higher class vessels (PC3 → PC1). The corresponding changes according to the simplified mechanics models are considerably milder.

In order to relate to the local pressures, the design local pressure was calculated in accordance with the IACS requirements, Section I2.3.2.2 (hull areas other than the bow). To account for scatter in the pressure values along the hull, the calculated design pressure value in the non-bow area was scaled by the Hull Area Factor (AF). Thus, for a ship with a given displacement and Polar Class a design pressure range is produced in the nonbow areas based on the maximum AF and minimum AF according to the IACS requirements. For the 'mechanics' model, the aspect ratio a_r was set to 3.6, which is equivalent to that in IACS Section I2.3.2.2. From the rectangular load patch of the IACS requirements, the contact height (corresponds to the contact area) was utilized to calculate the average pressure. It was assumed that the contact would start from

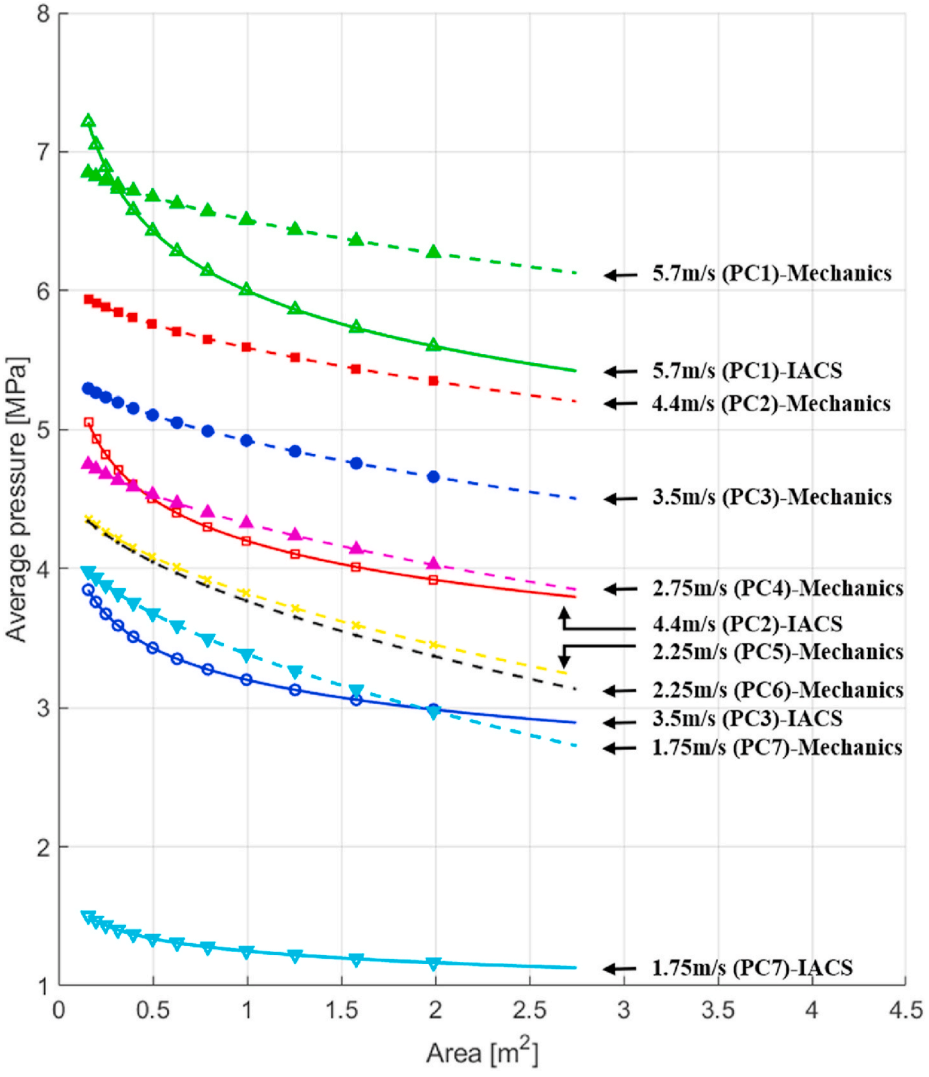

Fig. 4. Global pressures according to the IACS UR (*solid line with hollow markers*) and this study (*dashed line with solid markers*). The curves refer to velocities associated with the various Polar Classes.

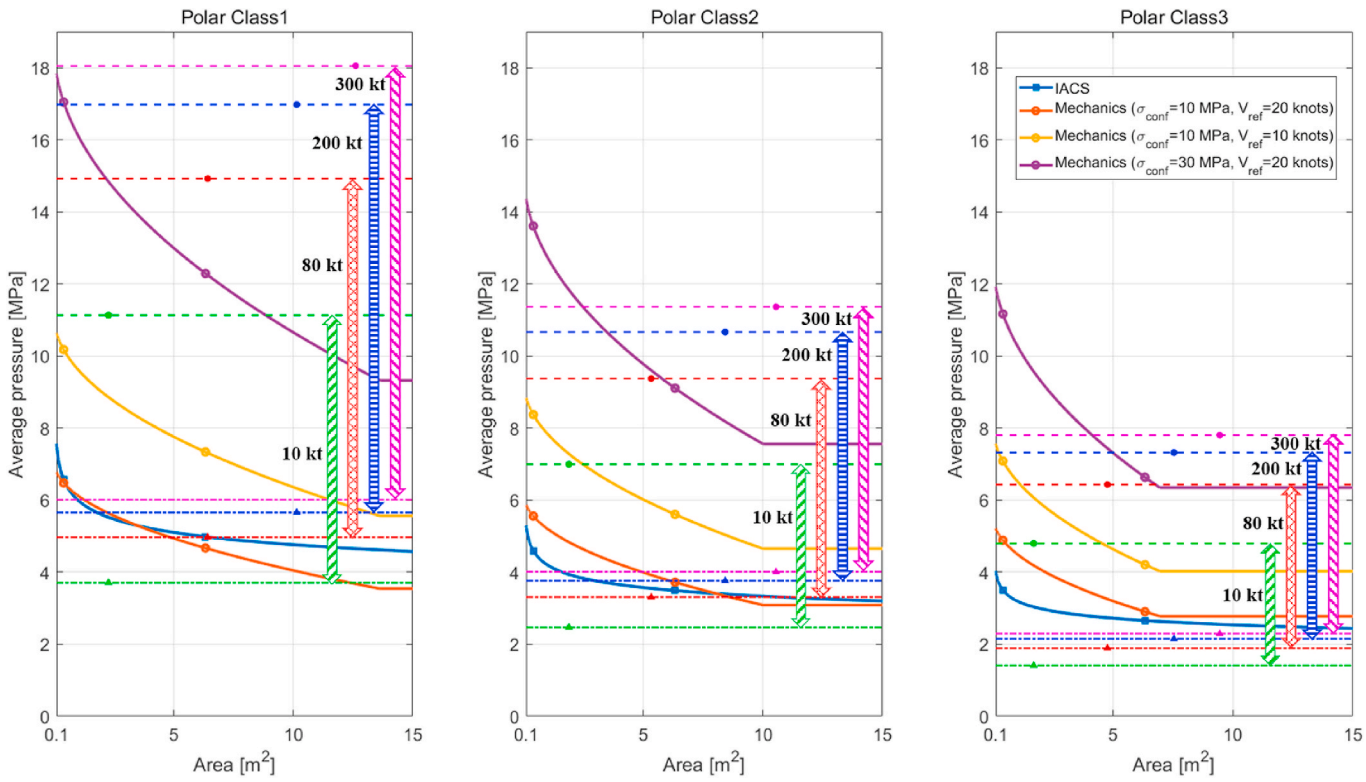

Fig. 5. Local pressures (dot markers) for nonbow areas according to IACS for PC1 to PC3 and this study. *Solid lines with square markers* and *circle markers* represent the pressure/area curves of IACS (process PA assumed) and the pressure/area curves of this study ('mechanics' model), respectively. The *red curve* corresponds to the 'mechanics' model with parameters listed in Table 1. From right to left for one class, the design pressure range of ships with displacements of 300 kt, 200 kt, 80 kt and 10 kt is displayed by *patterned arrows*. The *horizontal dashed lines* are used to place the pressures from the IACS rules in the context of those from the ice mechanics model (For interpretation of the references to color in this figure legend, the reader is referred to the Web version of this article.)

the middle of the contact thickness (a conservative estimate). Fig. 5 presents a local pressure/area from the IACS requirements for ships with PC1 to PC3 (hull areas other than the bow) and from the 'mechanics' model.

In the IACS requirements, as the size of the vessel increases, the upper limit, lower limit, and range of design pressure change. The same trend was observed with respect to the higher ice classes. This finding clearly indicates an increase in uncertainty when the ice class and/or vessel class increases.

Fig. 6 presents the speed effect on the local design pressure according

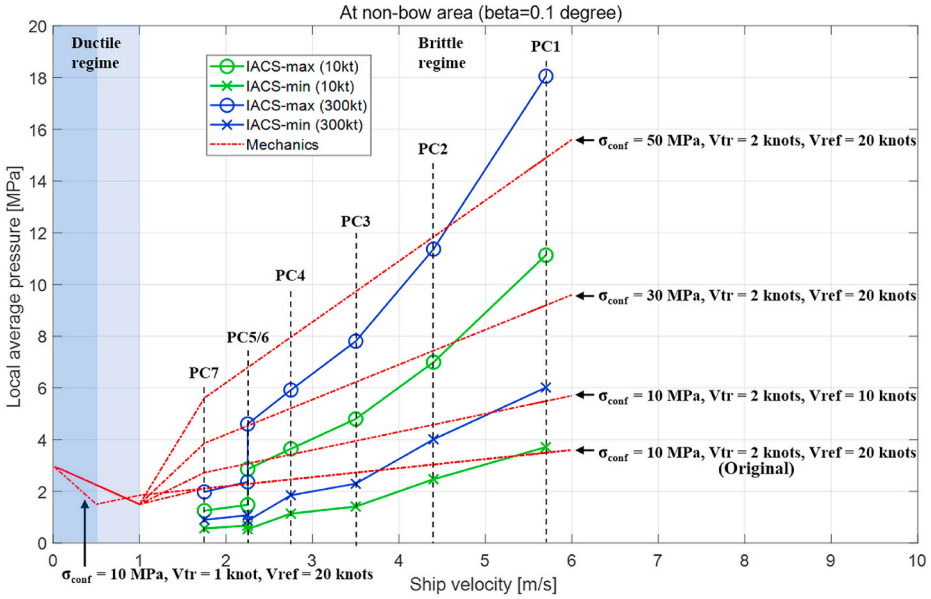

Fig. 6. Speed effects on the design pressure for nonbow areas. The *curves with circle markers* correspond to the maximum design pressure and the *curve with cross markers* denotes the minimum design pressure. The *dotted-dashed line* denotes the pressure from this study. The 'original' curve was produced using parameters in Table 1. The *left dark regime* is the ductile regime, and the *right white regime* is the brittle regime.

to IACS (Section I2.3.2.2) and the 'mechanics' model for two vessels (10 kt and 300 kt). For a ship with a given displacement and Polar Class, a design pressure range is produced in the nonbow areas based on the maximum AF and the minimum AF according to the IACS requirements. In the IACS requirements, the speed effect is considered a Polar Class attribute, so the relationship is discrete. The local pressures from the 'mechanics' model (Fig. 6) comprise the averaged pressure that corresponds to the full thickness (at the end of the penetration process). The relationship between design pressure and velocity is continuous, so the speed effect is milder and more linear than that in IACS. Furthermore, there is a large difference between pressures for higher ice classes (factor of 5 for PC1 at 6.0 m/s).

7. Discussion

In this paper, we have approached the uncertainties in rule-derived ice crushing loads from an ice mechanics point of view coupled with structural design considerations in a deterministic way. We have rederived the ice pressure-area relationships using simplified fundamental principles of ice strength and related them to those in the existing ship rules and recommendations (for nearly vertical structures, i.e., nonbow areas, where the effect of ice bending is minimized). For regions other than nonbow areas, where the effect of bending can be significant, Jordaan (2001) pointed out that the inclusion of flexural failure can improve the agreement between the calculated load data (based on random pressure-area coefficients) and the empirical load data.

Fig. 7 presents the conceptual difference between the crushing pressure representation in this study and that in IACS, RMRS (nonstandard hull shapes), and MHDM. In the ductile regime, the 'mechanics' approach considers a trapezoidal pressure profile with a zone of the constant pressures over a certain region, whereas the viscous extrusion approaches by Kurdyumov and Kheisin (1974) and by Kennedy et al. (1994) suggest a bell-shaped pressure profiles. When coupled with the structural design considerations (e.g., for plate thickness design, a localized loaded area is needed in the order of stiffener spacing squared), deviations from a nonuniform distributions will be less significant over the smaller areas. And if the peak pressures are not well pronounced over the loaded area (like in the ductile regime) the assumption of the uniform pressure profile is reasonable. In addition, Kurdyumov and Kheisn (1974) state that the pressure distribution in their model is close to uniform and it is reasonable to replace is with a constant pressure value.

In this study, spalling of ice (as a reduction in the contact area) was not considered. However, experimental evidence (e.g., Glen and Comfort, 1983) suggests that the actual contact area reduces as the speed increases. If this reduction is included in the 'mechanics' model, the average pressure will decrease at a faster rate with an increase in the contact area for higher velocities. Ductile ice strength depends on confinement and the loading rate. The triaxial ductile compressive strength of columnar-grained ice, which possesses the S2 growth texture (i.e., the across-column compressive strength measured under biaxial compressive loading across the columns and compressive loading along the columns of ice, whose crystallographic c-axes are confined to the horizontal plane of the ice cover but randomly oriented within this plane) is not affected by the along-column stresses (Schulson and Duval, 2009). Thus, the assumption of a uniform pressure distribution over h_i is reasonable.

The confined pressure value (Eq. (4c)) incorporates the resistance to fast crack growth K_{IC}, which is derived from the assumption of the universal behavior of brittle materials in compression (Renshaw and Schulson, 2001). This assumption is not applicable to the region of very high confinement, where plastic faulting operates. The pressure value corresponds to a central zone of the ice $s = 0.1$ m, which is also similar to the minimum stiffener spacing value. For smaller highly confined areas (where plastic faulting is activated), the experimental results (Jordaan, 2001) show a maximum pressure of 50 MPa. Furthermore, as the contact area tends to 0, the ice pressure has a physical limit that is equal to the theoretical ice strength of $0.1E$, where E is the Young's modulus of ice. Since the theoretical strength of steel is higher than that of ice, the latter will always fail first. Thus, on very small contact areas (order of mm $\times$ mm), pressures higher than σ_{peak} can occur. From a structural design point of view, the minimum relevant area for local design is equal to the stiffener spacing squared. This result is on the order of the sample size in the laboratory. Thus, the pressure for a contact area of 0.1×0.1 m^2 is unlikely to exceed that measured in the laboratory for freshwater, granular, 'nearly pure' ice samples in fully confined conditions.

Depending on the confinement, the ductile to brittle transition of salt-water ice at -10 °C occurs at a strain rate of approximately 10^{-3} 1/s (Schulson and Duval, 2009), which may be less than the assumed transition speed of 2.0 knots. A reference strain rate ($\approx V_{tr}/4B$) for $V_{tr} = 2$ knots is between $8 \cdot 10^{-4}$ and $5 \cdot 10^{-3}$, depending on the ship's dimension B [300 m, 50 m] and assuming that it acts as a moving indenter under idealized conditions (perfectly vertical structure, uniform contact areas, etc.). On the other hand, a vessel is generally designed to move continuously at a minimum steady speed of approximately 2.0 knots. At speeds less than 2.0 knots, the maneuverability of a vessel in ice will be lost and the vessel can become stuck in the ice. In the latter case, the ice-structure interaction is no longer governed by the vessel speed but is governed by the speed of the drifting ice. The speed of the latter could be low enough to impart ductile behavior over a design area. As the ice starts to build up around the vessel, which creates biaxial loading conditions, the presented model may be unconservative because it assumes that the ductile pressure is independent of the confinement. As noted in Schulson and Duval (2009), the ductile-to-brittle transition occurs gradually rather than abruptly, i.e., ductile-to-brittle transition occurs over a small range of strain rates instead of abruptly at a specific strain

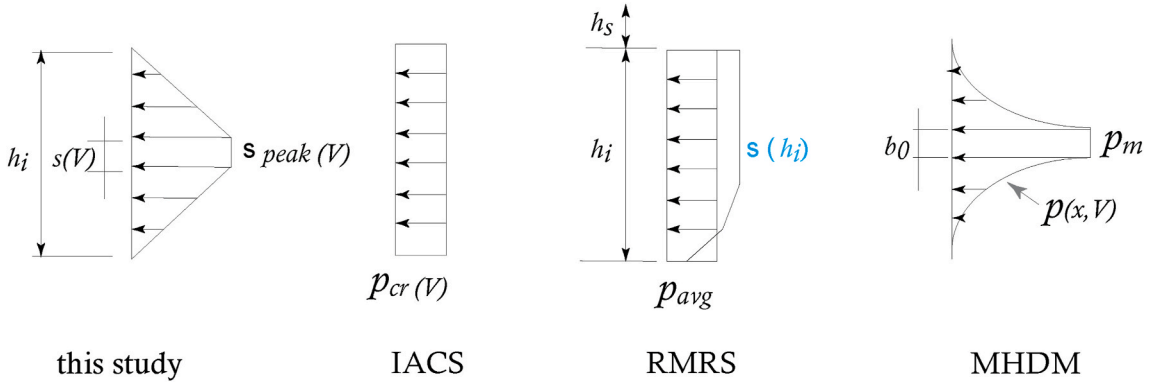

Fig. 7. Crushing pressure representation by different models: h_i is the ice thickness; h_s – snow thickness; p_{avg} – average pressure; V – vessel speed; p_{cr} – crushing pressure given by Equation (1); p_m, b_0 – parameters in Equation (3), $s(V)$ and $\sigma_{peak}(V)$ – parameters in Equations (4a)–(4d).

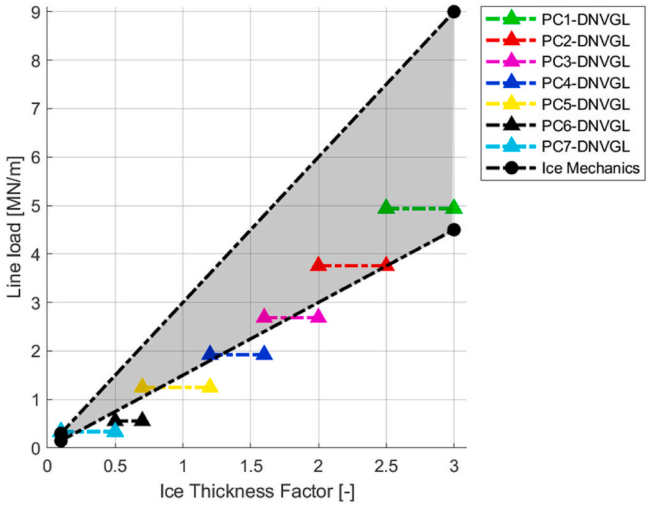

Fig. 8. Comparison between the ice compression load amidships in DNV GL rules (Section 6, pt. 4.8) and this study for the vertical side shell. The *dashed line with triangular markers* and *dashed line with circle markers* represent the line load values based on the DNV GL requirements and 'mechanics' model, respectively. The *colored area* corresponds to the design line load range of the 'mechanics' model (upper line corresponds to pressure over h_i = ice thickness factor, and lower line corresponds to pressure $h_i = 0.5 \times$ (ice thickness factor)).

rate. This occurrence is, however, not considered in detail. Furthermore, we have assumed that there is no speed effect on σ_{duct}.

A grain-size-dependent behavior is not considered. The characteristic grain size is chosen to be 10 mm (at least 10 grains across the highly confined region). Arguments for this choice is that grain-size effects will be less pronounced at engineering scale (m-scale) because of the imperfections (internal cracks, brine-pockets, and brine-drainage channels), temperature gradients, snow cover, etc.

The parameters for the ice mechanics approach (except V_{tr} and V_{ref}) are based on controlled laboratory and medium-scale tests. The ice pressure profile given by the 'mechanics' approach represents the limit state of the ice. Qualitatively, the results of this model agree with the experimental results of Sodhi et al. (1998), i.e., the local pressure (σ_{peak}) is higher at higher speeds than at lower speeds, whereas the average pressures can be higher in the ductile regime.

The results of the 'mechanics' model in the ductile regime have been placed in the context of the DNV GL ice compression load amidships (DNV GL AS, 2020, Section 6, pt. 4.8); refer to Fig. 8. For each Polar Class, the design line load for vertical side shells was calculated assuming that a ship is trapped between moving ice floes. Fig. 8 plots the load values as a function of the ice thickness factor. In the ductile regime, the functional dependency resembles that given by the DNV GL AS. However, regarding the load magnitude, the comparison is difficult because the pressure from the 'mechanics' model was converted to a line load assuming that the actual load height scales are proportional to the ice thickness factors (given in DNV GL, Section 6, pt. 4.8), but the exact relationship is uncertain.

We evaluated the 'mechanics' approach for different values of ductile-to-brittle transition speed (V_{tr}), reference speed (V_{ref}), and peak pressure (σ_{peak}). The results are plotted in Figs. 3, 5 and 6. The speed dependency given by the ice mechanics model is milder than that assumed in IACS, especially for the higher ice classes (PC2 and PC1). Even with σ_{peak} of 30–50 MPa—which is *three to five times greater* than the level recorded in the laboratory on freshwater, granular, 'nearly pure' ice samples in fully confined conditions—the pressure values given by IACS Section I2.3.2.2 for PC1 are higher (refer to Fig. 6).

Comparison of pressures in the ductile regime with design pressures (Fig. 6) indicates that smaller vessels with class below PC4 could receive side damage if they are stuck in ice, because the slow loading from 0.0 upwards will yield a higher average pressure than assumed in the design. To further investigate this scenario, the value of the ductile strength would need an additional calibration. In the above comparison, it should be taken into account that the considered IACS requirements do not explicitly specify ice temperature nor distinguish between summer – winter navigational seasons whereas the calculated pressures form the 'mechanics' model was based on −10 °C and may not include all the effects as the design formulations.

Regarding the IACS process pressure-area curve (Equation (1), $\beta = 10.1°$), flexural ice failure would have to be included in the 'mechanics model to further comment on the disparities observed in Fig. 4.

The IACS pressure values for the nonbow areas (shown in Figs. 5 and 6), which correspond to the higher ice classes (PC2 and PC1), seems to be very uncertain when the speeds of the larger vessels are considered. By imposing clear requirements that regulate the speeds of the vessel in ice, the uncertainty that was applied to the ice loads could be reduced. However, an entire ship hull (and flexural failure) should be considered instead of focusing on a specific area (crushing ice loads, nonbow area, IACS Section I2.3.2.2, in this study).

8. Concluding remarks

Currently, interpretations based on full-scale data (i.e., semi-empirical approaches) provide the best estimates of ice pressures on ship structures. This study lays the foundation for how to address the uncertainty in the rule-derived ice loads using the first principles of ice mechanics. The focus has been the local ice crushing load in IACS (nonbow areas), the process pressure area relationship $p = P_0 A^q$ ($q = -0.1$, P_0 depends on ice class), and speed effects. A pressure model was derived as a function of vessel speed and then plotted on the same figure as the pressure valued from the IACS approach. The derived model is based on simplified principles of ice mechanics that are coupled with design considerations. The main results of this study are summarized as follows:

Within the dominating brittle and brittle-like (i.e., plastic faulting) failure domain, the mechanics model exhibits trends that are similar to those assumed by IACS (i.e., increase in average pressure with increasing speed). If ice failure against an inclined ship side is concerned, the choice of q and P_0 appears to be reasonable. The choice of the parameters in the IACS Section I2.3.2.2 for nonbow areas, including the area factors for higher ice classes is, however, highly uncertain, especially for larger PC2 and PC1 vessels. Conversely, the smaller ice class vessels (<PC4) could be prone to side damage if ductile behavior of ice occurs (e.g., when the vessel is stuck in ice).

The presented approach could be expanded to other hull areas by accounting for flexural failure. The approach is based on observations at loading speeds that are slower when compared to ship-ice interactions. Despite a similar appearance of ice crushing processes in laboratory and in-situ, the presented approach could be refined in the future. Furthermore, it could be interesting to investigate if a probabilistic approach to ice loads and/or viscous extrusion approach could also be employed to address the uncertainty in the rule-derived ice loads. There is a need for full-scale ice data collection programs that not only focus on ice loads and underlying ice parameters but also incorporate human aspects (e.g., captain experience and decisions) and seek their 'risky' combinations w. r.t to vessel damage and the corresponding probability of occurrence.

CRediT authorship contribution statement

Ekaterina Kim: Writing – original draft, Conceptualization, Methodology, Visualization, Investigation, Supervision. **Jørgen Amdahl:** Supervision, Validation, Writing – review & editing. **Xintong Wang:** Visualization, Investigation, Validation, Writing – review & editing.

Declaration of competing interest

The authors declare that they have no known competing financial interests or personal relationships that could have appeared to influence the work reported in this paper.

Acknowledgements

The authors are grateful to Prof. Erland Schulson for his comments on this study. We are also grateful to anonymous reviewers for their valuable suggestions and comments, which helped to improve the work.

Appendix

MHDM

An analytical expression for the pressure profile over the loading height for the case of ice edge crushing is given in Appolonov et al. (2018). Some underlying assumptions are reported in Appolonov et al. (2011); however, a full derivation is not available in the published literature. This section presents a step-by-step derivation procedure.

The modified hydrodynamic model first assumes that there is an intermediate layer of crushed ice between the ship side and the solid undamaged ice. A basic relationship that relates the pressure (p) to the crushed layer thickness (h) is derived (refer to Eq. (A1)).

$$h^3\frac{\partial^2 p}{\partial x^2}+3h^2\frac{\partial p}{\partial x}\frac{\partial h}{\partial x}=-3\mu u_{pn} \tag{A1}$$

In Eq. (A1), μ is the dynamic viscosity of crushed ice in the intermediate layer, h is the thickness of the intermediate layer, and u_{pn} is the instantaneous ship speed.

To this point, the basic assumptions of the layer behavior are similar to those of Kurdyumov and Kheisin (1974, 1976); details of the derivation are presented in Kim and Amdahl (2016), and thus, are omitted here.

Next, MHDM assumes that the thickness of the intermediate crushed layer is linearly proportional to x (a vertical coordinate with the origin at the center of the loading height).

$$h=Kx. \tag{A2}$$

The following boundary conditions are introduced:

$$p(x=0.5b_0)=p_m \tag{A3}$$

$$p(x=0.5b)=0$$

Substituting Eq. (A2) into Eq. (A1) yields the following equation:

$$x^3\frac{\partial^2 p}{\partial x^2}+3x^2\frac{\partial p}{\partial x}=-3\mu u_{pn}\frac{1}{K^3} \tag{A4}$$

Equation (A4) can be rearranged to yield Eq. (A5). Using the integrating factor $m(x)$, Eq. (6) is obtained.

$$\frac{\partial^2 p}{\partial x^2}+\frac{3}{x}\frac{\partial p}{\partial x}=-3\mu u_{pn}\frac{1}{K^3}\frac{1}{x^3};\ m(x)=e^{\int\frac{3}{x}dx}=e^{3\ln|x|}=x^3 \tag{A5}$$

$$\frac{\partial}{\partial x}\left(\frac{\partial p}{\partial x}x^3\right)=-Au_{pn} \tag{A6}$$

Here, $A=3\mu\frac{1}{K^3}$.

Equation (A6) becomes

$$p=\frac{Au_{pn}}{x}-\frac{C_1}{2x^2}+C_2 \tag{A7}$$

Determine C_1 and C_2 by accounting for the boundary conditions expressed in Eq. (A3). Hence,

$$p=\frac{Au_{pn}}{x}-\frac{2Au_{pn}\left(\frac{1}{b}-\frac{1}{b_0}\right)+p_m}{4x^2\left(\frac{1}{b^2}-\frac{1}{b_0^2}\right)}+\frac{2Au_{pn}\left(\frac{1}{b}-\frac{1}{b_0}\right)+p_m}{b^2\left(\frac{1}{b^2}-\frac{1}{b_0^2}\right)}-\frac{2Au_{pn}}{b} \tag{A8}$$

$$p=\frac{2Au_{pn}}{b}\left(\frac{b}{2x}-1\right)+p_m\frac{b_0^2\left(b^2-4x^2\right)}{4x^2\left(b^2-b_0^2\right)}+\frac{2Au_{pn}}{b}\frac{b_0\left(4x^2-b^2\right)}{4x^2\left(b+b_0\right)} \tag{A9}$$

Equation (A9) is similar to the Appolonov solution, which is given in Eq. (A10).

$$p=\left[p_m-\frac{2Au_{pn}}{b}\left(\frac{b}{b_0}-1\right)\right]\frac{\left(\frac{b}{2x}\right)^2-1}{\left(\frac{b}{b_0}\right)^2-1}+\frac{2Au_{pn}}{b}\left(\frac{b}{2x}-1\right) \tag{A10}$$

Approach of RMRS (2017): An example calculation

The current method enables calculation of ice loads on ships and floating structures with nonstandard hull shapes. A detailed description is provided in RMRS (2017). The method is split into two parts: calculation of ice strength characteristics (RMRS, Section 3) and determination of ice loads (RMRS, Section 4). The approach to the calculation of ice loads conceptually follows that of Popov et al. (1967), and thus, is omitted herein. We only present an illustration of the approach to ice strength characterization based on the following conditions: winter-spring navigation (March) in the Kara Sea, first-year ice with a maximum thickness (h_i) of 1.45 m, and ice edge crushing against a vertical side structure.

The approach is empirical and enables site-specific applications. The local ice resistance to crushing is assumed to be a function of the uniaxial compressive strength. The latter depends on the show thickness, ice age (first year ice, multiyear ice), navigational season, ice temperature, salinity, and porosity. Details of the calculations are presented in the following paragraphs.

For the given ice thickness, a snow depth (h_s) of 0.2 m is applied. The equivalent ice thickness (h_{eq}) becomes $h_{eq} = h_i + 5h_s = 2.45$ m; refer to RMRS, Section 3.1.2, Eq. 3.4 for details.

Assume a nonlinear temperature distribution through the equivalent thickness in the form of Eq. (A11); refer to RMRS, Section 3.1.2, Eq. 3.6.

$$T(\bar{\delta}) = a + b\bar{\delta} + c\bar{\delta}^2 + d\bar{\delta}^3 \tag{A11}$$

In Eq. (A11), $\bar{\delta}$ is the normalized distance from the upper boundary of the snow-ice cover, which is calculated as $\bar{\delta} = \delta/h_{eq}$ (δ is a vertical distance between the upper boundary of the snow cover and the point of interest).

To reconstruct the temperature profile of the distribution through the equivalent ice thickness, four temperature values (at the reference points $\bar{\delta}$ = [0 0.5 0.75 1]) are calculated:

1. Minimal air temperature at the show surface: $T_{\min}$ ($\bar{\delta}$=0) = −40 °C (a monthly varying value).
2. Ice temperature in the middle of the equivalent ice thickness T ($\bar{\delta}$=0.5) = $0.5T_{avg}$ = −16.25 °C, where T_{avg} is the monthly average temperature of air for the previous month (March) for ice. T_{avg} = −32.5 °C is the average minimum temperature for the past five days.
3. T ($\bar{\delta}$=0.75) = 0.4 (0.5 T_{avg} + T_0) = −6.9 °C.
4. Ice temperature at the bottom of the ice sheet T_0 ($\bar{\delta}$=1) = −1 °C (freezing temperature of water).

Using the four pairs of ($\bar{\delta}$, T), the coefficients *a-d* in Eq. (A11) are calculated using curve fitting in MATLAB.

$$T(\bar{\delta}) = -40 + 48.93\bar{\delta} + 4.2\bar{\delta}^2 - 14.13\bar{\delta}^3 \tag{A12}$$

Equation (A12) is then adjusted for the ice thickness ($\bar{\delta} = \delta/h_i$) and becomes

$$T(\bar{\delta}) = -20.29 + 26.81\bar{\delta} - 4.591\bar{\delta}^2 - 2.93\bar{\delta}^3. \tag{A13}$$

Next, the salinity (S) distribution through the normalized ice thickness ($\bar{\delta}$) is calculated as

$$\frac{S}{S(avg)} = -0.2239\bar{\delta}^4 + 3.1592\bar{\delta}^3 - 1.6035\bar{\delta}^2 - 1.336\bar{\delta} + 1.45 \quad S(avg) = -4.606 + \frac{0.91693}{h_{ice}} \tag{A14}$$

where *S(avg)* denotes the average salinity over the ice thickness (in ppt); for details refer to RMRS, Section 3.2.1.

The porosity is expressed as the sum of the gas phase (v_a) and the liquid phase (v_b) (Eq. (A15))

$$v = v_a + v_b \; v_a = \frac{\rho S}{f_1(T)} f_2(T) \; v_b = \frac{\rho S}{f_1(T)} \tag{A15}$$

where ρ is the ice density (ρ = 920 kg/m3, RMRS, Section 3.2.2.1, Eq. 3.15). $f_1(T)$ and $f_2(T)$ are plotted in Figure A1 and are functions of temperature; refer to RMRS, Section 3.2.2).

The uniaxial compressive strength of first-year ice depends on the loading direction. For a horizontally loaded ice sheet, the strength is calculated using Eq. (A16) and expressed in MPa.

$$\left(\sigma_{comp}\right)_H = 10.1e^{-0.008v} \tag{A16}$$

For crushing against a vertical side structure, the average local contact pressure (p, MPa) is determined by Eq. (A17)

$$p = 2.4 \left(\sigma_{comp}\right)_H^{0.6} \tag{A17}$$

To ensure correct interpretation of the RMRS document, the calculated strength values were compared with those given in RMRS (2017), Section 3.3. Figure A2 presents the results of the calculations.

The local pressure (in Eq. (A17)) corresponds to contact areas in the order of 0.1–0.15 m^2. For larger contact areas, this pressure is scaled by factor (k), as shown in Eq. (A18). This factor depends on the width of the contact area $2\xi\tan(\phi/2)$, where ξ is the crushing depth and ϕ is the ice edge waterplane opening angle.

$$k = 0.7853e^{\left(-\frac{2\xi\tan\left(\frac{\phi}{2}\right)}{1.99}\right)} + 0.2146 \tag{A18}$$

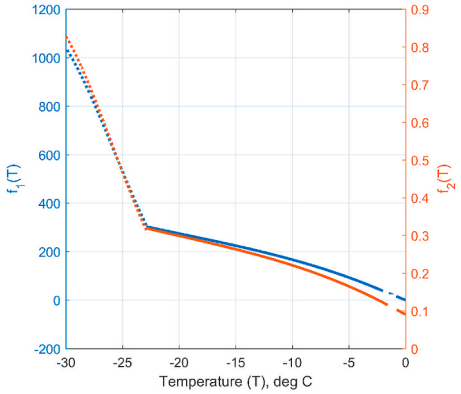

Fig. A1. Plot of f_1 and f_2 as a function of temperature

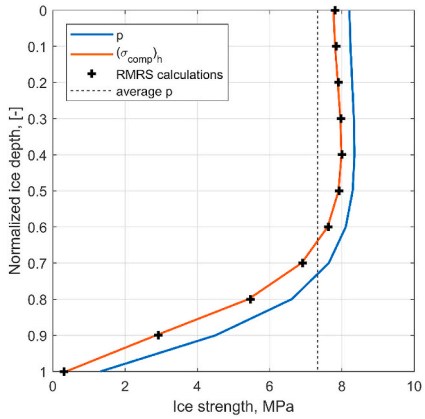

Fig. A2. Ice strength profiles of the distribution through the ice thickness in accordance with the RMRS methodology (p is the average local contact pressure; $(\sigma_{comp})_h$ is the uniaxial compressive strength for a horizontally loaded ice sheet).

Furthermore, in the calculations of the design pressure, an effective contact area is introduced, within which the pressure is considered constant and beyond which the pressure is assumed to be zero.

References

Appolonov, E.M., Didkovsky, A.V., Kuteinikov, M.A., Nesterov, A.B., 2011. Improvement in design models for ice load evaluation under vessel impact against ice. Ships Offshore Struct. 6 (3), 249–256.

Appolonov, E.M., Platonov, V.V., Tryaskin, V.N., 2018. Improvement of RMRS ice strengthening requirements for ice class vessels and icebreakers. Transactions of the Krylov State Research Centre 3 (385), 18–28 (in Russian).

Cho, S., Choi, K., 2019. Local ice load prediction formulas based on Arctic field measurements of the IBRV ARAON. Proceedings of the International Conference on Port and Ocean Engineering under Arctic Conditions. Port and Ocean Engineering under Arctic Conditions (POAC).

Daley, C., 2000. Background Notes to Design Ice Loads. IACS Ad-Hoc Group on Polar Class Ships. Transport Canada.

Frederking, R., 1998. The pressure area relation in the definition of ice forces. In: Proc. Of the 8th International Offshore and Polar Engineering Conference, vol. 2, pp. 431–437. Montreal.

Frederking, R., 1999. The local pressure-area relation in ship impact with ice. In: Proc. Of the 15th International Conference on Port and Ocean Engineering under Arctic Conditions, vol. 2, pp. 687–696. Helsinki.

Frederking, R., 2000. Local Ice Pressures from the Louis S. St Laurent 1994 North Pole Transit. National Research Council Report HYD-CR-054. Canadian Hydraulics Centre, Ottawa.

Geotech Arctic Services, 1985. Medium Scale Iceberg Impact Simulation Test Program. Report prepared for Mobil Oil Canada, Ltd.. CHC 20-37.

Glen, I.F., Blount, H., 1984. Measurements of ice impact pressures and loads onboard CCGS Louis S. St. Laurent. In: Proceedings of the 3rd Offshore Mechanics and Arctic Engineering Symposium, vol. 3, pp. 246–252.

Glen, I., Comfort, G., 1983. Ice impact pressure and load: investigation by laboratory experiments and ship trials. In: Proc. 7th. Int. Conf. On Port and Ocean Engineering under Arctic Conditions (POAC), vol. I, pp. 516–533. Helsinki.

Hänninen, S., Lensu, M., Riska, K., 2001. Analysis of the Ice Load Measurements during USCGC Healy Ice Trials, Spring 2000. Helsinki University of Technology, Espoo, Finland.

IACS, 2011. Unified Requirements for Polar Ships: I2–Structural Requirements for Polar Class Ships. International Association of Classification Societies.

IACS, 2019. History Files (HF) and Technical Background (TB) Documents for URs Concerning Polar Class (UR I). International Association of Classification Societies.

ISO 19906, 2018. Petroleum and Natural Gas Industries—Arctic Offshore Structures, second ed. International Standard, Geneva, Switzerland.

Iyerusalimskiy, A., Choi, J., Park, G., Kim, Y., Yu, H., 2011. The interim results of the long-term ice loads monitoring on the large Arctic tanker. In: Proc. Of the 21st International Conference on Port and Ocean Engineering under Arctic Conditions. POAC11-088.

Jo, Y., Choi, J., Park, S., Lee, J., Ki, H., Han, S., 2018. Comparison study between design ice load and actual measured ice load during ice trial of Arctic LNG carrier. In: Offshore Technology Conference.

Johansson, B.M., 1967. On the ice-strengthening of ship hulls. International Shipbuilding Progress; Shipbuilding and Marine Engineering Monthly 14 (154).

Jordaan, I.J., 2001. Mechanics of ice-structure interaction. Eng. Fract. Mech. 68 (17–18), 1923–1960.

Kennedy, K.P., Jordaan, I.J., Maes, M.A., Prodanovic, A., 1994. Dynamic activity in medium-scale ice indentation tests. Cold Reg. Sci. Technol. 22 (3), 253–267.

Kim, E., Amdahl, J., 2016. Discussion of assumptions behind rule-based ice loads due to crushing. Ocean. Eng. 119.

Kim, E., Schulson, E.M., 2015. A phenomenological explanation of the pressure-area relationship for the indentation of ice: two size effects in spherical indentation experiments. Cold Reg. Sci. Technol. 115.

Kim, T.-W., Kim, H.-N., Choi, K., Lee, T.-K., 2014. Study on Influence of Ship Speed on Local Ice Loads on Bow of the IBRV ARAON. International Society of Offshore and Polar Engineers.

Kim, H., Dolny, J., Quinton, B., Yu, H., Peng, H., 2016. Characterization of full scale operational ice pressures and hull response on a large Arctic tanker. Offshore Technology Conference. https://doi.org/10.4043/27408-MS.

Kotisalo, K., Kujala, P., 1999. Ice load measurements onboard MT Uikku during the ARCDEV voyage. In: Tuhkuri, J., Riska, K. (Eds.), POAC'99. Proceedings of the 15th International Conference on Port and Ocean Engineering under Arctic Conditions, vol. 3, pp. 974–987.

Kujala, P., Vuorio, J., 1986. Results and Statistical Analysis of Ice Load Measurements Onboard Icebreaker SISU in Winters 1979 to 1985. Winter Navigation Research Board, Helsinki. Research Report 43.
Kurdyumov, V.A., Kheisin, D.E., 1974. About definition of ice loads acting on ice-breaker hull under impact. Proc. Leningr. Shipbuild. Inst. 90, 95–100 (in Russian).
Kurdyumov, V.A., Kheisin, D.E., 1976. Hydrodynamic model of the impact of a solid ice. Pricladnaya Mech 12 (10), 103–109 (in Russian).
Kwon, Y.-H., Lee, T.-K., Choi, K., 2015. A study on measurements of local ice pressure for ice breaking research vessel "ARAON" at the Amundsen Sea. International Journal of Naval Architecture and Ocean Engineering 7 (3), 490–499.
Matsuzawa, T., Takimoto, T., Shimoda, H., Wako, D., 2010. Five-year observations of ship hull ice load in the Southern Sea of Okhotsk. In: 20th IAHR International Symposium on Ice; Jun 14–18. Lahti, Finland.
Popov, Y., Fadeyev, O., Kheisin, D., Yakovlev, A., 1967. Strength of Ships Sailing in Ice. Sudostroenie Publishing House, Leningrad, p. 223 (in Russian).
Ralph, F.E., 2016. Design of Ships and Offshore Structures: a Probabilistic Approach for Multi-Year Ice and Iceberg Impact Loads for Decision-Making with Uncertainty. Doctoral (PhD) thesis. Memorial University of Newfoundland.
Register, Lloyd's, 2015. House of Lords Evidence Submission ARC0048.
Renshaw, C.E., Schulson, E.M., 2001. Universal behavior in compressive failure of brittle materials. Nature 412 (6850), 897–900.
Riska, R., 2018. Ice edge failure process and modelling ice pressure. Phil. Trans. Math. Phys. Eng. Sci. 376 (2129).
Riska, K., Kämäräinen, J., 2011. A review of ice loading and the evolution of the Finnish–Swedish Ice Class Rules. Trans. - Soc. Nav. Archit. Mar. Eng. 119, 265–298.
Ritch, R., Frederking, R., Johnston, M., Browne, R., Ralph, F., 2008. Local ice pressures measured on a strain gauge panel during the CCGS Terry Fox bergy bit impact study. Cold Reg. Sci. Technol. 52 (1), 29–49.
RMRS, 2017. Methods for Calculating Ice Loads on Vessels and Floating Structures Whose Hull Shape Differs from that Regulated by RS Rules, ND 2-139902-030, Russian Maritime Register of Shipping (in Russian).
Schulson, E.M., Duval, P., 2009. Creep and Fracture of Ice. Cambridge University Press, p. 401.
Sodhi, D., Takeuchi, T., Nakazawa, N., Akagawa, S., Saeki, H., 1998. Medium-scale indentation tests on sea ice at various speeds. Cold Reg. Sci. Technol. 28, 161–182.
St John, J.W., Minnick, P.V., 1995. Ice Load Impact Study on the National Science Foundation's Research Vessel Nathaniel B. Palmer. Report No. SSC-376.
St John, J.W., Daley, C., Blount, H., 1990. Ice Loads and Ship Response to Ice-Summer 1982/winter 1983 Test Program. Report No. SSC-329.
Timco, G.W., Sudom, D., 2013. Revisiting the Sanderson pressure–area curve: defining parameters that influence ice pressure. Cold Reg. Sci. Technol. 95, 53–66.
Kurdyumov, V.A., Tryaskin, V.N., Kheisin, D.E., 1980. Определение ледовой прочности корпусов транспортных судов. Научно-технический сборник, Регистр СССР Вып.9: Теоретические и практические вопросы прочности и конструкции Морских судов, 42-48. (In Russian).